An Adaptive Sliding Mode Controller for a PAM-based Actuator

Quy-Thinh Dao
School of Electrical and Electronic Engineering, Hanoi University of Science and Technology, Vietnam
thinh.daoquy@hust.edu.vn

Vuong Van Dinh
Hanoi University of Science and Technology, Vietnam | Hanoi Vocational College of High Technology, Vietnam
vuongdv@hht.edu.vn

Chien Tuan Vu
Hanoi University of Science and Technology, Vietnam
chien.vt181355@sis.hust.edu.vn

Thuyet Quang Pham
Hanoi University of Science and Technology, Vietnam
thuyet.pq181778@sis.hust.edu.vn

Duc Minh Duong
Hanoi University of Science and Technology, Vietnam
duc.duongminh@hust.edu.vn
(corresponding author)

Received: 5 December 2022 | Revised: 20 December 2022 | Accepted: 23 December 2022

ABSTRACT

The Pneumatic Artificial Muscle (PAM) is a promising actuator for developing the human-robot interaction system. However, modeling and controlling PAM-based actuators are a significant difficulty due to the inherent uncertainty and hysteresis of PAM. Besides, the control approach of a PAM-based system also deals with unknown disturbances that always exist in any system. This study developed a sliding mode controller that employs an adaptive law to deal with issues and improve control performance. Furthermore, the stability of the proposed controller is proven based on the Lyapunov stability criterion. Finally, through a series of tests, the effectiveness of the proposed control approach is verified.

Keywords-pneumatic artificial muscle; sliding mode control; adaptive law; antagonistic configuration

I. INTRODUCTION

Robotics industry has grown rapidly during the recent years, especially regarding robots that move in the same way as humans do. PAM is a potential actuator mechanism that responds to this tendency, because it can stretch in the same way that human muscles can. Besides its flexibility in movement, is possesses benefits such as high power-to-weight, ease of maintenance, inherent safety, and low cost [1-5]. The above characteristics have made PAM a special research object, with common applications including manipulators, robotic orthosis, etc. [6-13]. However, controlling PAM faces many challenges. The deviation in mathematical model estimation and the sensitivity to external disturbances are obstacles that need to be overcome if the PAM control is to achieve optimal performance. Many algorithms have been proposed to solve the control problem for this actuator, such as the traditional PID controller and its enhanced variations [14-19]. Nevertheless, the above controllers show limitations for the hysteresis and nonlinear characteristics of PAM. Nonlinear controllers to address the limitations of PID controllers, such as the fuzzy controller [20, 21], the neural network based controller [22], and the nonlinear ADRC controller [23], have been employed in several recent studies. In addition, the sliding mode controller and its various versions are always the leading candidates for the tasks of controlling nonlinear objects [17,

24-27]. Nonetheless, PAM is a nonlinear object, and the parameter estimation for the model of the PAM-based system is approximate and if the system disturbance is very high, it definitely affects the control quality of the aforementioned methods. As a result, creating a disturbance observer will aid in overcoming PAM's restrictions. In this study, a disturbance observer based on the adaptive law is developed to not only estimate the system disturbance component accurately but also to help the controller adapt to sudden external influences affecting the PAM system. As a result, control performance is improved. The effectiveness of the employed control approach is verified by experiments under different conditions. In addition, the stability of the overall system is proven by Lyapunov theory.

II. SYSTEM DESCRIPTION

The system structure consists of two artificial muscles in antagonistic setup as shown in Figure 1. Two PAMs are supplied from an air compressor through two proportional valves (SMC, ITV-2030-212S-X26). One muscle bundle contracts while the other relaxes when the artificial muscle system is inflated and deflated through two proportional valves, causing the pulley to revolve about its axis of rotation. A potentiometer (WDD35D8T) measures the rotational angle produced. For software, the proposed controller is programmed on an education controller type from National Instrument (myRIO-1900). The controller calculates the potentiometer's feedback angle value and sends the control output to the electric control valves. LabVIEW software is used to monitor the entire procedure.

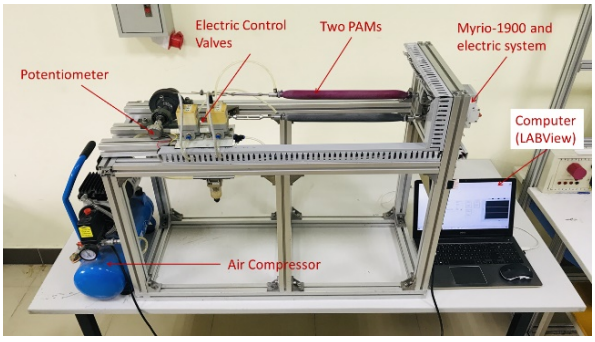

Fig. 1. The PAM-based experiment platform.

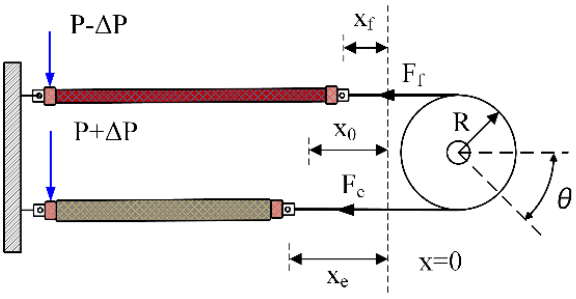

Fig. 2. The working principle of PAM-based antagonistic configuration.

Figure 2 depicts the operating principle of the PAMs. The two muscles are simultaneously initialized with the same amount of gas at the same pressure $P_0 = 0.2$MPa, causing them to contract to the same position X_0. When the lower muscle bundle is injected with a pressurized amount of air ΔP and at the same time the upper muscle is reduced by a corresponding amount of air, the lengths of the two muscle bundles change as $X_0 - X_e$ and $X_0 - X_f$ respectively. As a result, the pulley rotates at an angle of θ. Therefore, controlling the change in air pressure inside the two muscles will result in a change in the pulley rotation angle. The internal pressure of both PAMs is obtained as follows:

$$\begin{cases} P_1 = P_0 + \Delta P \\ P_2 = P_0 - \Delta P \end{cases} \quad (1)$$

The control voltage of the proportional regulator valve PAM is determined using (1) as follows:

$$\begin{cases} u_1 = u_0 + u = k_0(P_0 + \Delta P) \\ u_2 = u_0 - u = k_0(P_0 - \Delta P) \end{cases} \quad (2)$$

where u_1 and u_2 are two voltages applied to two proportional regulator valves corresponding to the two PAMs, k is a constant indicating the voltage-pressure relationship on the valve, and u is the control variable that regulates the amount of pressure change ΔP because the rotation angle of the pulley is changed by altering the control output u of the two proportional valves. As a result, the control output u would be the only input variable, with the observed joint angle θ being the output. After introducing the disturbance, the discrete-time SISO model of the system can be expressed by:

$$y_k = -\sum_{i=0}^{n} a_i y_{k-i} + \sum_{j=0}^{m} b_j u_{k-j} + p_k \quad (3)$$

where u_k is the control output at instant k, y_k is the pulley's angle, p_k represents the system disturbances. The model parameters are a_i and b_j. In [17], the authors chose a second-order discrete-time model (with $m = n = 2$) and the least-squares method to determine the mathematical model for PAM. The coefficients of the model are shown in Table I.

TABLE I. MATHEMATICAL MODEL PARAMETERS

Parameter	Value
a_1	−1.9567 ± 0.0092
a_2	−0.9576 ± 0.0128
b_1	0.0126 ± 0.0013
b_2	0.0124 ± 0.0049

III. CONTROLLER DESIGN

The design of the Adaptive Sliding Mode Controller (ASMC) is described in this section. Firstly, the SMC is designed based on the sliding surface theory. The system's uncertainty disturbance component is then estimated using an adaptive law-based noise observer. As a result, the control quality of the SMC is improved. Finally, the controller is verified for stability based on the Lyapunov stability condition. Figure 3 illustrates the block diagram of the overall system. The recommended SMC is described in the next subsection.

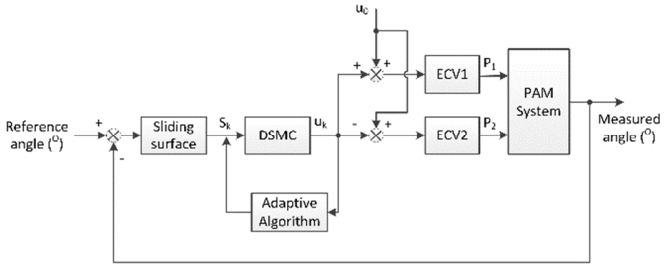

Fig. 3. Block diagram of the proposed control approach.

A. Sliding Mode Controller

Tracking deviation is determined by:

$$e_k = y_k^* - y_k \tag{4}$$

where y_k^* is the reference signal.

Consider a sliding surface as follows:

$$s_k = e_k + \alpha e_{k-1} \tag{5}$$

where α is the tuning parameter $0 < \alpha < 1$. Equation (5) is rewritten as:

$$s_k = y_k^* - y_k - \alpha e_{k-1} \tag{6}$$

Replacing y_k from (3) and (6) can be expressed as:

$$s_k = y_k^* + \sum_{i=0}^{n} a_i y_{k-1} - \sum_{j=0}^{m} b_j u_{k-j} - p_k + \alpha e_{k-1} \tag{7}$$

To ensure the sliding variable is driven on the sliding surface, the following reaching law is taken into consideration.

$$\Delta s_k = s_k - s_{k-1} = -K_{SW} sign(s_k) \tag{8}$$

or:

$$s_k = s_{k-1} - K_{SW} sign(s_k) \tag{9}$$

where $K_{sw} > 0$ is the control gain. By replacing s_k from (9) into (7), the control signal u_k becomes:

$$u_k = \frac{1}{b_1}[y_k^* + \sum_{i=1}^{n} a_i y_{k-i} - \sum_{j=0}^{m} b_j u_{k-j} - p_k + \alpha e_{k-1} - s_{k-1} + K_{SW} sign(s_k)] \tag{10}$$

Component p_k in u_k is a variable of the unknown system disturbance. As a result, we propose in this paper an observer that uses adaptive law to estimate that component, and thereby improving the efficiency of the SMC. Finally, with the estimated value $\hat{p}_k$ of p_k, the control signal u_k is calculated as:

$$u_k = \frac{1}{b_1}[y_k^* + \sum_{i=1}^{n} a_i y_{k-i} - \sum_{j=0}^{m} b_j u_{k-j} - \hat{p}_k + \alpha e_{k-1} - s_{k-1} + K_{SW} sign(s_k)] \tag{11}$$

The architecture of an adaptive law-based disturbance observer is examined in greater depth below.

B. Adaptive Algorithm

As previously stated, the unknown disturbance p_k has a significant impact on the control signal u_k. The proposed adaptive algorithm for estimating the p_k component improves the control signal's accuracy. The following is a presentation of the adaptive law:

$$\hat{p}_k = \hat{p}_{k-1} - \varphi s_k \tag{12}$$

where φ is a strictly positive constant related to the adaptation rate. It is clear that:

$$\Delta\hat{p}_k = \hat{p}_k - \hat{p}_{k-1} - \varphi s_k \tag{13}$$

Equation (13) also shows that there is no adaptation when states are on the sliding surface:

$$\Delta\hat{p}_k = 0 \quad \text{for } s_k = 0 \tag{14}$$

C. Stable Analysis of Adaptive Sliding Mode Controller

This subsection presents the stability analysis of the proposed controller using the Lyapunov stability condition. It allows the ASMC's parameter to be determined. Consider the error value of the actual system disturbance component and the estimated component of the observer.

$$\tilde{p}_k = p_k - \hat{p}_k \tag{15}$$

It is obvious that:

$$\Delta\tilde{p}_k = \Delta p_k - \Delta\hat{p}_k \tag{16}$$

When the sliding surface variable s is 0, (14) indicates that there won't be any adaptation, resulting in the following calculation of $\Delta\tilde{p}_k$:

$$\Delta\tilde{p}_k = -\Delta\hat{p}_k = \varphi s_k \tag{17}$$

The following Lyapunov function is used as the base for the stability proof of the proposed controller:

$$V_k = \frac{1}{2} s_k^2 + \frac{1}{2\varphi} \tilde{p}_k^2 \tag{18}$$

Hence, we have:

$$\Delta V_k = V_k - V_{k-1} = \frac{1}{2} s_k^2 - \frac{1}{2} s_{k-1}^2 + \frac{1}{2\varphi} \tilde{p}_k^2 - \frac{1}{2\varphi} \tilde{p}_{k-1}^2 \tag{19}$$

Consider the following expression:

$$\Delta_s = \frac{1}{2} s_k^2 - \frac{1}{2} s_{k-1}^2 = \Delta s_k s_k - \frac{1}{2} (\Delta s_k)^2 \tag{20}$$

On the other hand, Δs_k is represented as:

$$\Delta s_k = s_k - s_{k-1} = y_k^* + \sum_{i=1}^{n} a_i y_{k-i} - \sum_{j=0}^{m} b_j u_{k-j} - p_k + \alpha e_{k-1} - s_{k-1} \tag{21}$$

Substituting u_k from (11) into (21) we get:

$$\Delta s_k = -\tilde{p}_k - K_{SW} sign(s_k) \quad (22)$$

Then, (20) becomes:

$$\Delta_s = \left[-\tilde{p}_k - K_{SW} sign(s_k)\right] s_k - \frac{1}{2}(\Delta s_k)^2 = -\tilde{p}_k s_k - K_{SW} sign(s_k) s_k - \frac{1}{2}(\Delta s_k)^2 \quad (23)$$

Next, we consider the following expression:

$$\Delta_p = \frac{1}{2\varphi}\tilde{p}_k^2 - \frac{1}{2\varphi}\tilde{p}_{k-1}^2 = \frac{1}{\varphi}\Delta\tilde{p}_k.\tilde{p}_k - \frac{1}{2\varphi}\left(\Delta\tilde{p}_k\right)^2 \quad (24)$$

Replacing $\Delta\tilde{p}_k = \varphi s_k$ into (24), we obtain:

$$\Delta_p = \frac{1}{\varphi}\Delta\tilde{p}_k.\tilde{p}_k - \frac{1}{2\varphi}\left(\Delta\tilde{p}_k\right)^2 = \tilde{p}_k s_k - \frac{1}{2\varphi}\left(\Delta\tilde{p}_k\right)^2 \quad (25)$$

From (19), (23), and (25) we have:

$$\Delta V_k = \Delta_s + \Delta_p$$

$$= -\tilde{p}_k s_k - K_{SW} sign(s_k) s_k - \frac{1}{2}(\Delta s_k)^2 + \tilde{p}_k s_k - \frac{1}{2\varphi}\left(\Delta\tilde{p}_k\right)^2$$

$$= -K_{SW} sign(s_k) s_k - \frac{1}{2}(\Delta s_k)^2 - \frac{1}{2\varphi}\left(\Delta\tilde{p}_k\right)^2 \le 0$$

Thus, the system is asymptotically stable.

IV. EXPERIMENTAL RESULTS

A series of different circumstances is conducted to verify the effectiveness of the proposed ASMC controller. The experiment uses two types of input signals: pure-sine and mixed-sine trajectories, as follows:

$$f(t) = 20\sin 2\pi f \quad (24)$$

$$f(t) = 20\sin 2\pi f + 12.8\sin \pi f \quad (25)$$

These types of signals change frequency, from 0.1Hz to 0.8Hz, during the experiments. Furthermore, the system is evaluated with two scenarios, with load and no-load, for each input signal at a certain frequency. With the sample time T_s of 5ms, the control algorithm will be built using the LabVIEW/MyRIO toolbox and then incorporated into the MyRIO-1900 controller. On the LabVIEW interface, the whole motion trajectory of the object will be measured and presented. The conventional SMC is used as a counterpart to demonstrate the proposed controller's usefulness. Table II shows the parameters of the ASMC and SMC after fine-tuning.

Below the system is tested to track pure-sine orbitals with frequency varying between 0.1 and 0.8Hz. The analytical evaluation will show the advantages of tracking the performance of ASMC than of SMC. A load of 5.0kg also is added to the system to evaluate the robustness of the system when there are external disturbances. In subsection *B*, the same test scenarios and evaluations as subsection *A* are repeated. However, the input signal will be mixed-sine orbitals to test the capabilities of ASMC compared to SMC.

TABLE II. ADSMC AND DSMC PARAMETERS

Parameters	k_{SW}	α	φ
ASMC	0.5	0.1	0.04
SMC	0.75	0.1	

A. Experiment with Pure-Sinusoidal Reference Signal

The system is evaluated when tracking pure-sine wave signals with frequencies ranging from 0.1 to 0.8Hz. The system operates with both load and no-load situations for each input signal. For example, Figure 4 demonstrates the experimental results when the system tracks 0.1 and 0.5Hz desired signals without a load. It can be seen that, at zero load, the tracking performance of ASMC is better than SMC's, especially in the steady state. Particularly, the maximum deviation values of ASMC and SMC at 0.1Hz are about 1.0° and 3.0°, respectively. Meanwhile, the performance of two controllers at 0.5Hz are 3.0 and 4.0°, respectively. There is no significant difference between the two controllers at the transient state.

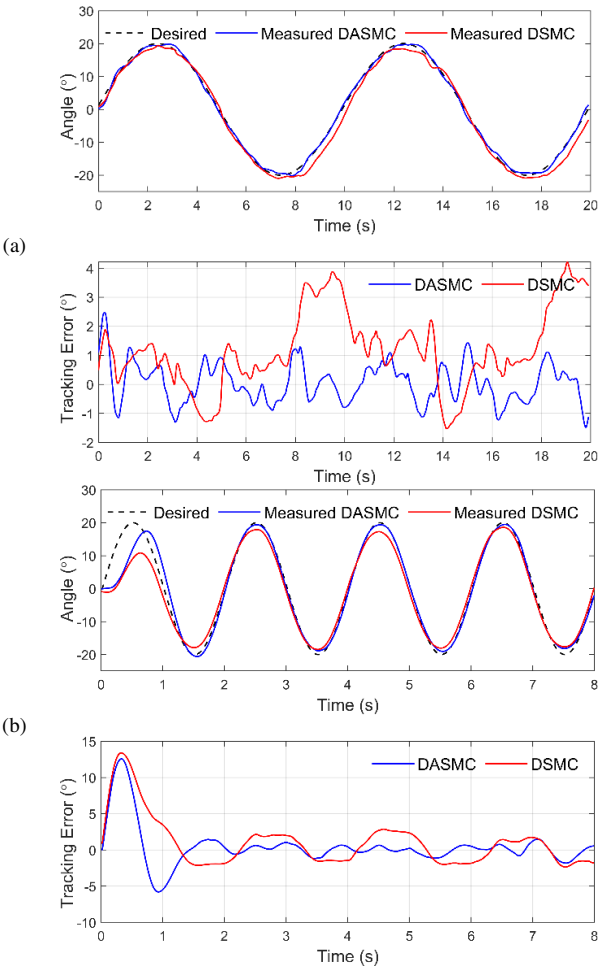

Fig. 4. Experiment results for tracking a pure-sinusoidal signal without a load: (a) 0.1Hz, (b) 0.5Hz.

With the system under loaded scenario in Figure 5, we observe that both controllers are affected. However, ASMC still outperforms SMC in terms of tracking performance. In

more detail, the highest deviation values for SMC and SMC at 0.1 Hz are 2.0 and 4.0°, respectively. The tracking performance of both controllers is lowered at 0.5Hz, with the highest errors of 4.5 and 5.0°, respectively. Table III shows the RMSE of the two controllers under the first scenarios experiment.

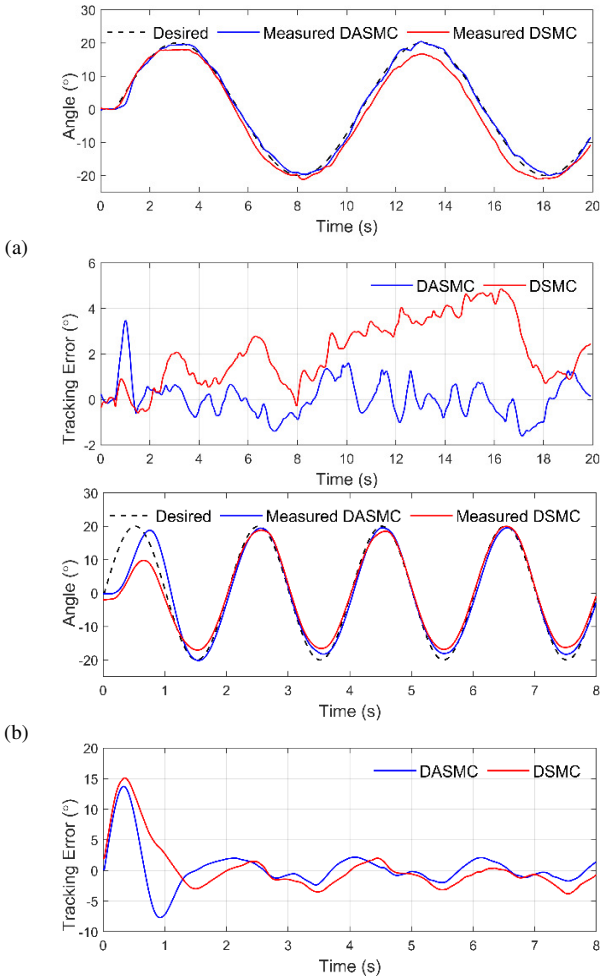

Fig. 5. Experiment results for tracking a pure sinusoidal trajectory with a load (m = 5.0kg): (a) 0.1Hz, (b) 0.5Hz.

B. Experiment with Mixed-Sine Reference Signal

Finally, ASMC and SMC are tested with mixed-sine orbital input. Figures 6 and 7 depict the tracking performance results of the two controllers when the system is tested under no-load and loaded conditions, respectively. In the case of no-load scenario, although the trajectory is more complicated, SAMC still performs well in terms of tracking, in contrast to SMC. It is observed that the response rate of SMC is slower than the change of the orbital reference signal. For example, at 0.25Hz, ASMC's highest deviation value is 3.0°, while SMC's is 6.0°. At 0.4Hz, the maximum error value of the two controllers is 4.0 and 7.0°, respectively. When the system had a load, the general trend of the two controllers is still to show reduced tracking performance, but ASMC still shows its ability in orbit tracking.

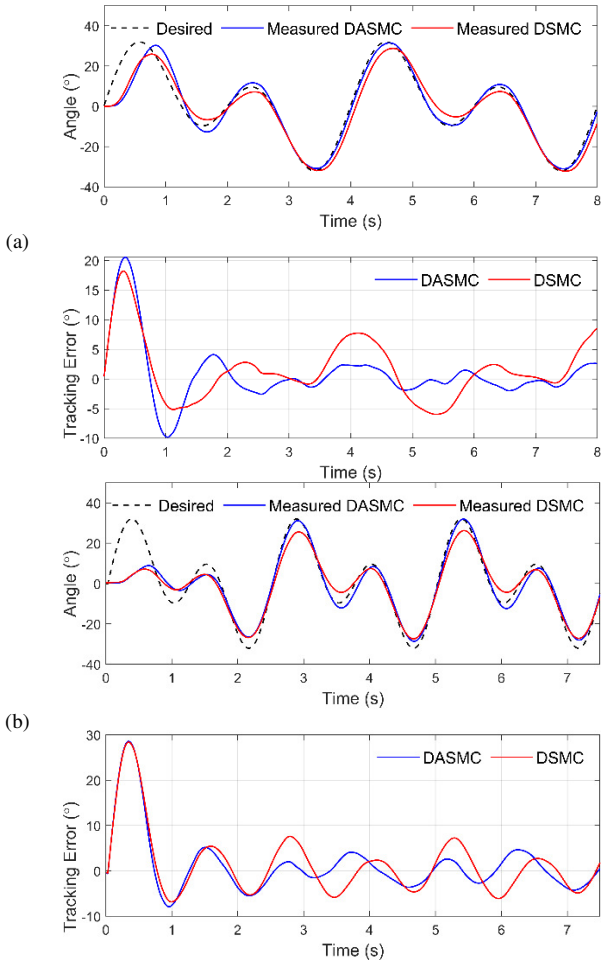

Fig. 6. The results of the experiments for tracking a mixed sinusoidal trajectory without a load:(a) 0.25Hz, (b) 0.4Hz.

TABLE III. RMSE OF THE TWO CONTROLLERS WITH SINUSOIDAL ORBITAL SIGNAL

	Frequency (Hz)	**Without load**		**Load m = 5kg**	
		ASMC	**SMC**	**ASMC**	**SMC**
Pure-sine signal	0.1	0.7	1.8	0.8	2.5
	0.5	2.8	3.5	3.3	3.9
	0.8	3.9	5.0	4.1	5.2
Mixed-sine signal	0.05	0.9	1.9	0.9	2.0
	0.25	5.0	5.9	5.5	6.4
	0.4	6.6	7.1	6.7	7.3

In both pure-sine and mixed-sine trajectories, with or without load, the ASMC always shows advantages over the conventional SMC. The proposed adaptive algorithm has observed the disturbance successfully. Thus, the disturbance is rejected, and the tracking performance is increased significantly. In the case of sudden load change, the driving trajectory of the PAM under the control of ASMC almost immediately returns to the steady-state as before the load changed. Moreover, in a load scenario with a pure sinusoidal input signal at low frequency (0.1Hz), the RMSE value of ASMC is only 1.0°, while that of traditional SMC is larger (2.0°). With mixed-sine trajectories, the results are the same. In

terms of 0.4Hz frequency trajectories, the ASMC has a RMSE value of 6.0°, which is lower than the RMSE value of the traditional SMC (7.0°). However, the ASMC still has the limitation that the transient time is larger than that of the traditional SMC. This is a common disadvantage of adaptive controllers because it takes a certain amount of time to update the value of the parameter it estimates. The ASMC still shows outstanding performance in the steady state in all experimental scenarios.

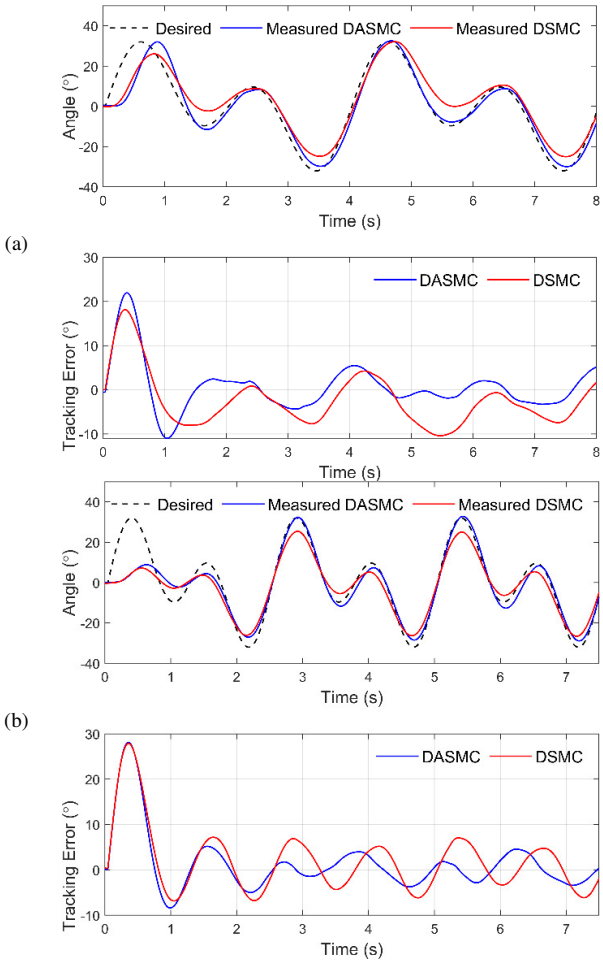

Fig. 7. Experiment results for tracking a mixed sinusoidal trajectory with a load (m = 5.0 kg): (a) 0.25Hz, (b) 0.4Hz.

V. CONCLUSION

This paper proposes a sliding mode controller with an adaptive disturbance observer for a PAM-based actuator. The proposed adaptive sliding mode control shows accuracy quality in orbit tracking, and good adaptability to external disturbances. Those qualities are all verified through different test scenarios with pure-sine and mixed-sine input signals at the frequency range from 0.05 to 0.8Hz. The adaptive algorithm helps to accurately estimate the system noise, thereby improving the control quality of conventional sliding mode controllers. Because of the disturbance observation process, the transient time of ASMC is larger than that of the traditional SMC. The ASMC still shows outstanding performance in the steady state in all experimental scenarios. In following research, solutions to speed up the disturbance estimation will be studied in order to shorten the transient process for the proposed controller, thereby helping the controller to show better quality in the two aspects of transient and steady-state times for PAM.

ACKNOWLEDGMENT

This research is funded by the Hanoi University of Science and Technology (HUST) under project number T2022-PC-002.

REFERENCES

[1] F. Daerden and D. Lefeber, "Pneumatic artificial muscles: Actuators for robotics and automation," *European Journal of Mechanical and Environmental Engineering*, vol. 47, no. 1, pp. 11–21, 2002.

[2] C.-P. Chou and B. Hannaford, "Measurement and modeling of McKibben pneumatic artificial muscles," *IEEE Transactions on Robotics and Automation*, vol. 12, no. 1, pp. 90–102, Oct. 1996, https://doi.org/10.1109/70.481753.

[3] M. Sekine, K. Shiota, K. Kita, A. Namiki, and W. Yu, "A lightweight shoulder prosthesis with antagonistic impact-absorbing hybrid actuation for bimanual activities of daily living," *Advances in Mechanical Engineering*, vol. 8, no. 4, pp. 1–17, Apr. 2016, https://doi.org/10.1177/1687814016645982.

[4] K. K. Aun and H. P. H. Anh, "System Modeling Identification and Control of the Two-Link Pneumatic Artificial Muscle Manipulator Optimized with Genetic Algorithms," in *IEEE International Conference on Control and Automation*, Guangzhou, China, Jun. 2007, pp. 501–506, https://doi.org/10.1109/ICCA.2007.4376407.

[5] C.-J. Chiang and Y.-C. Chen, "Neural network fuzzy sliding mode control of pneumatic muscle actuators," *Engineering Applications of Artificial Intelligence*, vol. 65, pp. 68–86, Oct. 2017, https://doi.org/10.1016/j.engappai.2017.06.021.

[6] I. D. Walker, "Continuous Backbone 'Continuum' Robot Manipulators," *International Scholarly Research Notices*, vol. 2013, Jul. 2013, Art. no. e726506, https://doi.org/10.5402/2013/726506.

[7] T.-Y. Choi and J.-J. Lee, "Control of Manipulator Using Pneumatic Muscles for Enhanced Safety," *IEEE Transactions on Industrial Electronics*, vol. 57, no. 8, pp. 2815–2825, Dec. 2010, https://doi.org/10.1109/TIE.2009.2036632.

[8] G. Kim, S. Kang, H. Cho, J. Ryu, M. Mun, and K. Kim, "Modeling and simulation of powered hip orthosis by pneumatic actuators," *International Journal of Control, Automation and Systems*, vol. 8, no. 1, pp. 59–66, Feb. 2010, https://doi.org/10.1007/s12555-010-0108-9.

[9] G. S. Sawicki and D. P. Ferris, "A pneumatically powered knee-ankle-foot orthosis (KAFO) with myoelectric activation and inhibition," *Journal of NeuroEngineering and Rehabilitation*, vol. 6, no. 1, Jun. 2009, Art. no. 23, https://doi.org/10.1186/1743-0003-6-23.

[10] S. Z. Ying, N. K. Al-Shammari, A. A. Faudzi, and Y. Sabzehmeidani, "Continuous Progressive Actuator Robot for Hand Rehabilitation," *Engineering, Technology & Applied Science Research*, vol. 10, no. 1, pp. 5276–5280, Feb. 2020, https://doi.org/10.48084/etasr.3212.

[11] P. Beyl *et al.*, "Safe and Compliant Guidance by a Powered Knee Exoskeleton for Robot-Assisted Rehabilitation of Gait," *Advanced Robotics*, vol. 25, no. 5, pp. 513–535, Jan. 2011, https://doi.org/10.1163/016918611X558225.

[12] S. Hussain, S. Q. Xie, and P. K. Jamwal, "Control of a robotic orthosis for gait rehabilitation," *Robotics and Autonomous Systems*, vol. 61, no. 9, pp. 911–919, Sep. 2013, https://doi.org/10.1016/j.robot.2013.01.007.

[13] D. Kim, Y.-P. Hong, and K.-S. Kim, "Bipedal Walking and Impact Reduction Algorithm for a Robot with Pneumatically Driven Knees," *International Journal of Control, Automation and Systems*, vol. 19, no. 12, pp. 3937–3946, Dec. 2021, https://doi.org/10.1007/s12555-020-0613-4.

[14] G. Andrikopoulos, G. Nikolakopoulos, and S. Manesis, "Non-linear control of Pneumatic Artificial Muscles," in *21st Mediterranean Conference on Control and Automation*, Platanias, Greece, Jun. 2013, pp. 729–734, https://doi.org/10.1109/MED.2013.6608804.

[15] K. K. Ahn and T. D. C. Thanh, "Nonlinear PID control to improve the control performance of the pneumatic artificial muscle manipulator using neural network," *Journal of Mechanical Science and Technology*, vol. 19, no. 1, pp. 106–115, Jan. 2005, https://doi.org/10.1007/BF02916109.

[16] D. Zhang, X. Zhao, and J. Han, "Active Model-Based Control for Pneumatic Artificial Muscle," *IEEE Transactions on Industrial Electronics*, vol. 64, no. 2, pp. 1686–1695, Oct. 2017, https://doi.org/10.1109/TIE.2016.2606080.

[17] Q.-T. Dao, D.-H. Mai, D.-K. Nguyen, and N.-T. Ly, "Adaptive Parameter Integral Sliding Mode Control of Pneumatic Artificial Muscles in Antagonistic Configuration," *Journal of Control, Automation and Electrical Systems*, vol. 33, no. 4, pp. 1116–1124, Aug. 2022, https://doi.org/10.1007/s40313-022-00902-5.

[18] T. Nuchkrua and T. Leephakpreeda, "Fuzzy Self-Tuning PID Control of Hydrogen-Driven Pneumatic Artificial Muscle Actuator," *Journal of Bionic Engineering*, vol. 10, no. 3, pp. 329–340, Sep. 2013, https://doi.org/10.1016/S1672-6529(13)60228-0.

[19] H. Wang and J. Lu, "Research on Fractional Order Fuzzy PID Control of the Pneumatic-hydraulic Upper Limb Rehabilitation Training System Based on PSO," *International Journal of Control, Automation and Systems*, vol. 20, no. 1, pp. 310–320, Jan. 2022, https://doi.org/10.1007/s12555-020-0847-1.

[20] A. Rezoug, F. Hamerlain, and M. Hamerlain, "Application of Fuzzy Sliding Mode to control of Manipulator Robot actuated by Pneumatic artificial Muscles," *IFAC Proceedings Volumes*, vol. 42, no. 19, pp. 580–585, Jan. 2009, https://doi.org/10.3182/20090921-3-TR-3005.00099.

[21] Z. Nadjat, B. Behih, Z. Bouchama, and K. Zehar, "Robust Adaptive Fuzzy Control of Nonlinear Systems," *Engineering, Technology & Applied Science Research*, vol. 12, pp. 8328–8334, Apr. 2022, https://doi.org/10.48084/etasr.4781.

[22] S. Tian, G. Ding, D. Yan, L. Lin, and M. Shi, "Nonlinear Controlling of Artificial Muscle System with Neural Networks," in *IEEE International Conference on Robotics and Biomimetics*, Shenyang, China, Aug. 2004, pp. 56–59, https://doi.org/10.1109/ROBIO.2004.1521751.

[23] K. Xing, J. Huang, Y. Wang, J. Wu, Q. Xu, and J. He, "Tracking control of pneumatic artificial muscle actuators based on sliding mode and non-linear disturbance observer," *IET Control Theory & Applications*, vol. 4, no. 10, pp. 2058–2070, Oct. 2010, https://doi.org/10.1049/iet-cta.2009.0555.

[24] J. H. Lilly and P. M. Quesada, "A two-input sliding-mode controller for a planar arm actuated by four pneumatic muscle groups," *IEEE Transactions on Neural Systems and Rehabilitation Engineering*, vol. 12, no. 3, pp. 349–359, Sep. 2004, https://doi.org/10.1109/TNSRE.2004.831490.

[25] D. M. Duc, T. X. Tuy, and P. D. Phuoc, "A Study on the Response of the Rehabilitation Lower Device using Sliding Mode Controller," *Engineering, Technology & Applied Science Research*, vol. 11, no. 4, pp. 7446–7451, Aug. 2021, https://doi.org/10.48084/etasr.4312.

[26] W. M. Bessa and R. S. S. Barreto, "Adaptive fuzzy sliding mode control of uncertain nonlinear systems," *Sba: Controle & Automação Sociedade Brasileira de Automatica*, vol. 21, pp. 117–126, Apr. 2010, https://doi.org/10.1590/S0103-17592010000200002.

[27] C. P. Vo, X. D. To, and K. K. Ahn, "A Novel Adaptive Gain Integral Terminal Sliding Mode Control Scheme of a Pneumatic Artificial Muscle System With Time-Delay Estimation," *IEEE Access*, vol. 7, pp. 141133–141143, 2019, https://doi.org/10.1109/ACCESS.2019.2944197.